Observation of room-temperature ballistic thermal conduction persisting over 8.3 μm in SiGe nanowires

Tzu-Kan Hsiao[1,2], Hsu-Kai Chang[3], Sz-Chian Liou[1], Ming-Wen Chu[1], Si-Chen Lee[3] and Chih-Wei Chang[1]*

In ballistic thermal conduction, the wave characteristics of phonons allow the transmission of energy without dissipation. However, the observation of ballistic heat transport at room temperature is challenging because of the short phonon mean free path. Here we show that ballistic thermal conduction persisting over 8.3 μm can be observed in SiGe nanowires with low thermal conductivity for a wide range of structural variations and alloy concentrations. We find that an unexpectedly low percentage (∼0.04%) of phonons carry out the heat conduction process in SiGe nanowires, and that the ballistic phonons display properties including non-additive thermal resistances in series, unconventional contact thermal resistance, and unusual robustness against external perturbations. These results, obtained in a model semiconductor, could enable wave-engineering of phonons and help to realize heat waveguides, terahertz phononic crystals and quantum phononic/thermoelectric devices ready to be integrated into existing silicon-based electronics.

The presence of phonon scattering processes and the associated complex interferences of phonons limit the wave characteristics within a phonon mean free path, l. The short mean free path ($l < 0.1$ μm) at room temperature for most materials has hindered the observation of ballistic thermal conduction. According to the kinetic theory of phonons, the thermal conductivity κ is given by

$$\kappa = \frac{1}{3} \sum_n C_n v_n l_n \tag{1}$$

where C_n is the volumetric specific heat, v_n is the average phonon velocity, l_n is the phonon mean free path of the nth phonon mode, and the sum is over all excited phonon modes. Equation (1) shows that materials displaying high κ will probably exhibit long l. Indeed, good thermal conductors such as nanotubes, graphene and diamond all exhibit long values of l (∼0.9 μm) at room temperature[1,2]. Unfortunately, these values are impractical for most phononic applications that need to exploit the wave properties of heat. Longer mean free paths can be achieved at low temperatures (<4 K) thanks to the removal of high-frequency phonons with short mean free paths. However, cryogenic setups are unsuitable for most phononic applications. These facts have so far limited the investigation of ballistic thermal conduction either at ultralow temperatures or in materials exhibiting high κ.

We note that not all excited phonons participate in the heat conduction processes, and the mean free paths are strongly frequency-dependent in equation (1). In our approach, instead of searching for high-κ materials or low temperatures, we investigate mechanisms that can efficiently filter out the highest-frequency phonons at room temperature. The remaining long-life, low-frequency phonons will display ballistic thermal conduction persisting for long distances.

Alloy scattering plays an important role in enhancing phononic and thermoelectric applications, and an abrupt decrease in κ can be observed when a small alloy concentration is introduced[3–6]. Alloy scattering originates from the random distributions of the different elements, with different mass, in an alloyed material. They are strongly frequency-dependent and can efficiently suppress the contribution from high-frequency optical phonons while leaving the low-frequency acoustic phonons unaffected[3–5]. However, although recent theoretical works have indicated $l > 1$ μm in alloys[3–5], no experimental measurements have directly tackled the evidence of ballistic thermal conduction or unravelled the efficiency of alloy scattering in filtering phonons under external perturbations. Here we provide experimental evidence of room-temperature ballistic thermal conduction in $Si_{1-x}Ge_x$ nanowires.

SiGe nanowires are a model alloy system in which the role of alloy scattering at nanoscale dimensions can be investigated thoroughly. A wide range of structural variation and alloy concentrations ($x \approx 0.1$–0.6) were generated using chemical vapour deposition methods (see Methods)[7,8]. To investigate the thermal conduction of individual SiGe nanowires, we fabricated microscale thermal conductivity test fixtures consisting of suspended heaters and sensors, as shown in Fig. 1a. Nanowires with selected lengths or diameters were picked up and placed on the test fixture by a sharpened tungsten tip operated by a piezo-driven manipulator inside a scanning electron microscope (SEM). *In situ* deposition of Pt/C composites was then carried out to rigidly bond the nanowire to the test fixture, as shown in Fig. 1b. The test fixture can be transferred to a transmission electron microscope (TEM) so that all geometric/structural/elemental information about the measured nanowires can be gathered. From the measured thermal conductance K, sample length L and cross-sectional area A, we can experimentally determine κ using the expression $\kappa = KL/A$ (see Methods and Supplementary Section S1). Figure 1c–f and g–j shows scanning TEM (STEM) images, high-resolution TEM images and elemental mappings based on energy-dispersive X-ray spectroscopy of two representative SiGe nanowires. It can be seen that the SiGe nanowires are homogeneously alloyed with compositions varying from $Si_{0.9}Ge_{0.1}$ to $Si_{0.4}Ge_{0.6}$. Notably, twin boundaries, stacking faults, striped compositional variations, and defects are present in the $Si_{0.4}Ge_{0.6}$ nanowires (Fig. 1g–j, Supplementary Section S2).

[1]Center for Condensed Matter Sciences, National Taiwan University, Taipei 10617, Taiwan, [2]Institute of Applied Physics, National Taiwan University, Taipei 10617, Taiwan, [3]Graduate Institute of Electronic Engineering, National Taiwan University, Taipei 10617, Taiwan. *e-mail: cwchang137@ntu.edu.tw
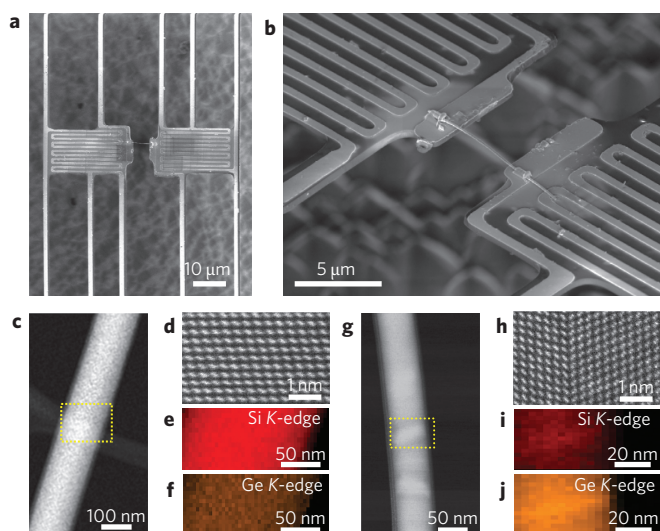
Figure 1 | Thermal conductivity test fixtures and structures of the SiGe nanowires. a, SEM image of a thermal conductivity test fixture consisting of suspended heater and sensor pads. **b**, Enlarged SEM image of **a** showing a SiGe nanowire anchored on the thermal conductivity test fixture. **c**, Representative STEM image of a homogeneously alloyed $Si_{0.9}Ge_{0.1}$ nanowire. **d**, Atomic-resolution image of **c** showing the crystalline lattice. **e,f**, Si and Ge K-edge elemental mappings of the area within the yellow-dotted rectangle in **c**, showing homogeneous Si and Ge distributions. **g**, Representative STEM image of a $Si_{0.4}Ge_{0.6}$ nanowire showing uniform intensity distributions radially and aperiodic striped distributions axially. **h**, Atomic-resolution image of **g** displaying a twin boundary. **i,j**, Si and Ge K-edge elemental mappings of the yellow-dotted rectangle in **g**, showing that Si and Ge elements are homogeneously alloyed with striped composition variations.

Ballistic thermal conduction over 8.3 μm

Classically, phonon propagation without scattering can, in principle, exhibit unlimited thermal conduction. However, it is not true in quantum mechanics, as Landauer's formulation dictates that even ballistic transport will carry finite quantum thermal conductance per channel, and thermal resistance will always occur whenever there are geometric restrictions on the number of quantum channels. Because ballistic thermal conduction indicates dissipationless heat transfer and geometric constrictions only occur at the contacts, the measured thermal conductivity κ should be linearly proportional to L (or, equivalently, $K = $ constant), and the corresponding contact thermal resistance will display the quantum nature for any two-probe measurements. Thus, l can be determined experimentally wherever the heat conduction transits from ballistic (that is, $\kappa \approx L$) to diffusive (that is, $\kappa = $ constant) regime in the κ versus L relation. We have experimentally measured the length dependence of κ for more than 20 SiGe nanowires of different diameters, structures and alloy concentrations. All data are plotted in Fig. 2.

Surprisingly, despite the variations between different SiGe nanowires, all the data in Fig. 2 clearly display a universal correlation between κ and L. Remarkably, the thermal conductivity of SiGe nanowires increases linearly with length, with a constant slope for $L < 8.3$ μm. Furthermore, the data falling on the dashed line of Fig. 2 extrapolates to $\kappa = 0$ when L approaches zero. The constant slope, the zero offset and $\kappa/L = K/A$ indicate that the thermal conductivity is zero (that is, finite thermal resistance) when L approaches zero, and the thermal resistance occurs exclusively at the contacts for $L < 8.3$ μm. This is consistent with the definition of ballistic thermal conduction described above and Landauer's formulation, whereby K is independent of L (or equivalently, $\kappa \approx L$) for
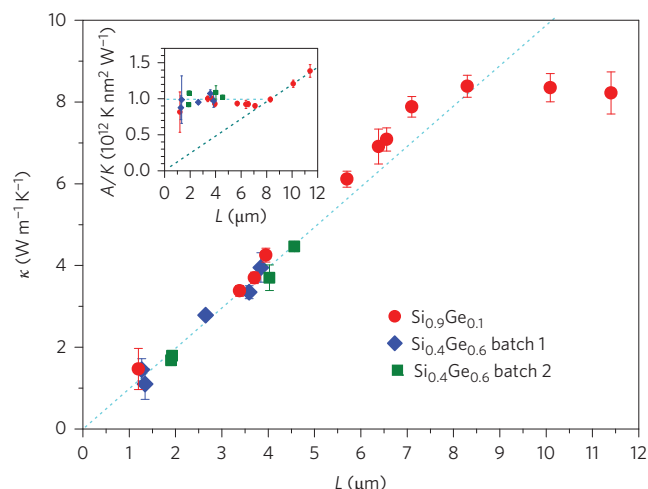

Figure 2 | κ versus L for more than 20 SiGe nanowires with different structures and alloy concentrations. The data for $L < 8.3$ μm all fall on a dashed line intersecting at the origin, indicating ballistic thermal conduction at room temperature in SiGe nanowires for a wide range of structures and concentrations. Inset: the same data plotted as thermal resistance per unit area (A/K) versus L. Note that extrapolating the data in the diffusive regime ($L > 8.3$ μm) to $L \rightarrow 0$ (blue dotted line) indicates negligible (classical) contact thermal resistance, whereas extrapolating the data in the ballistic regime ($L < 8.3$ μm) to $L \rightarrow 0$ (cyan dotted line) indicates constant (quantum) contact thermal resistance, which depends on the cross-sectional area A of the nanowires rather than the real contact area.

a ballistic thermal conductor[9]. On the other hand, for $L > 8.3$ μm, additional dissipation occurs inside the SiGe nanowires so that the heat conduction behaves like an ordinary diffusive thermal conductor (that is, $\kappa = $ constant), agreeing with previous results for bulk SiGe[10,11]. Therefore, Fig. 2 provides direct evidence of ballistic thermal conduction persisting for $l \approx 8.3$ μm, which is not only an unprecedentedly large value at room temperature, but is also more than nine times longer than the phonon mean free path of nanotubes, graphene or diamond[1,2]. Remarkably, the ultralong phonon mean free path is even longer than the electronic counterparts ($l_{electron} < 1$ μm) of the highest-mobility (>200,000 cm^2 V^{-1} s^{-1}) graphene devices[12,13].

Unconventional contact thermal resistance

Experimentally, the contact thermal resistance is defined as the measured thermal resistance as $L \rightarrow 0$. In the diffusive (classical) regime, contact thermal resistance results from the back-scattering of phonons. In the ballistic (quantum) regime, contact thermal resistance occurs even if the phonons are scattering-free, but the available quantum channels are geometrically constricted at the contacts. To observe the two distinct effects, we plot the data from Fig. 2 as thermal resistance per unit area (A/K) versus L in the inset of Fig. 2. Importantly, extrapolating the data in the diffusive regime ($L > 8.3$ μm) to $L \rightarrow 0$ gives negligible classical contact resistance (<2% of the thermal resistance of the nanowires), indicating nearly scattering-free transmission of phonons at the contacts. On the other hand, extrapolating the data in the ballistic regime ($L < 8.3$ μm) to $L \rightarrow 0$ shows that the contact thermal resistance ($1/K = L/A\kappa$) is inversely proportional to the cross-sectional area ($A = \pi d^2/4$) of the nanowire rather than the real contact area ($\sim \pi d L_c$, where $L_c \approx 300$ nm is the physical contact length of the nanowire and the heater/sensor pads, d is the diameter of the nanowire). This counter-intuitive result is in fact due to the geometric constriction of the available heat conduction channels in a ballistic thermal conductor[14]. Because the number of phonon modes of a
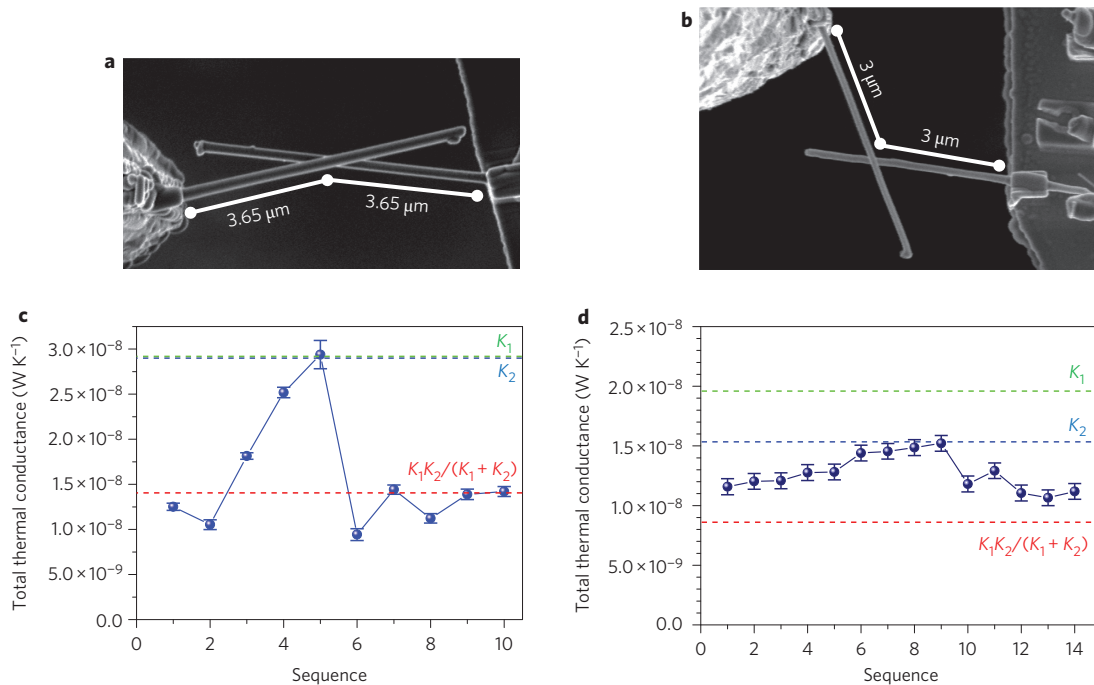
Figure 3 | Demonstration of non-additive thermal resistances in series. a,b, Representative SEM images of two SiGe nanowires of similar diameters ($d_1 \approx d_2$, $K_1 \approx K_2$) (**a**) and dissimilar diameters ($d_1 \neq d_2$, $K_1 \neq K_2$) (**b**) connected in series. **c,d,** Corresponding measured total thermal conductance K_{total} when the respective junction thermal resistance is varied sequentially by rubbing, pressing or rotating the two SiGe nanowires against each other using a manipulator (see Supplementary Fig. S6 for corresponding SEM images from the sequences). Green, blue and red dashed lines denote the values of K_1, K_2 and $K_1K_2/(K_1 + K_2)$, respectively. The blue/red dashed line also denotes the maximum K_{total} allowed from equation (2) for ballistic/diffusive thermal conductors. Note that the total lengths are within the ballistic thermal conduction regime ($L_1 + L_2 < 8.3\,\mu m$) for both systems. .

waveguide is constrained by the smallest cross-sectional area, considering that $\pi d^2/4 \ll \pi dL_c$ in our experiment, the total number of available channels for transmitting heat is thus limited by $\pi d^2/4$ rather than πdL_c. The effect also explains why such small deviations to the dashed line in Fig. 2 are observed for SiGe nanowires with different contact geometries. We have also conducted an experiment studying thermal resistance ($1/K$) versus L of an individual SiGe nanowire and concluded that the classical contact resistance contributes less than 10% of the total thermal resistance (Supplementary Section S3). Furthermore, independent analyses suggest that the classical contact thermal resistance must be less than 10%, otherwise the κ of SiGe nanowires would be larger than that of bulk SiGe[10,11].

The combination of large l and small κ is at odds with conventional beliefs that materials exhibiting low κ will have short l, which is now known to yield incorrect estimates that $l < 0.01\,\mu m$ for SiGe[10,15–17]. Nevertheless, our result is consistent with recent theoretical calculations that $l \approx 10\,\mu m$ for SiGe alloys[4]. In fact, theoretical calculations have indicated that the low-frequency acoustic phonons (<1 THz) are the dominant carriers in transmitting heat[5].

Because the low-frequency acoustic phonons are nearly dispersionless, simple yet surprising information can be derived from the slope ($\kappa/L = 9.5 \times 10^5$ W K^{-1} m^{-2}) of the dashed line in Fig. 2. From kinetic theory, $\kappa/L \approx C_a v_a/3$ (where C_a and $v_a = 4{,}108$ m s^{-1} are, respectively, the average specific heat and the average sound velocity of the low-frequency phonons), and we obtain $C_a = 680$ J K^{-1} m^{-3} and $C_a/C_{bulk} = 0.04\%$ (where $C_{bulk} = 1.7 \times 10^6$ J K^{-1} m^{-3} is the experimentally measured specific heat)[18]. Therefore, nearly 99.96% of the excited phonons are filtered out by alloy scattering, and the low-frequency phonons carrying out the heat conduction in the SiGe nanowires only occupy 0.04% of the excited phonon modes. Incorporating the density of states of SiGe[19], we further estimate that these phonons exhibit frequencies less than 0.3 THz (Supplementary

Section S4). On the other hand, applying similar analyses to Si and Ge[20,21], where alloy scattering is absent, reveals ~20–30% of the excited phonon modes are responsible for ballistic heat conduction (Supplementary Section S5). This result is consistent with theoretical calculations that show that phonons below 1 THz dominate the heat transfer in SiGe[5]. In contrast, phonons up to 6 THz contribute equally to the heat transfer in Si[5].

Quantum mechanically, the maximum heat flow per channel is limited by fundamental constants[9]. Applying the Landauer formulation of quantum thermal conductance to the dashed line in Fig. 2 indicates that each quantum channel occupies an average area of ~100 nm^2 (Supplementary Section S6). This result suggests that the dominant acoustic phonon wavelength is larger than 10 nm (or the frequency is less than 0.4 THz), which is again consistent with previous estimates.

Non-additive thermal resistances in series

Ballistic conduction also allows experimental demonstrations of the non-additive property of resistances in series, a phenomenon that was known, in the past, to occur exclusively in low-dimensional ballistic electronic systems at ultralow temperatures[22]. Similar to the electrical counterparts, connecting two diffusive or two ballistic thermal conductors in series is known to yield distinct results for the total thermal conductance K_{total}:

$$K_{total} \leq \begin{cases} (K_1, K_2)_{min} & \text{for ballistic conductors} \\ K_1 K_2/(K_1 + K_2) & \text{for diffusive conductors} \end{cases} \quad (2)$$

This inequality holds when the classical contact thermal resistance at the junction is non-zero. $(K_1, K_2)_{min}$ denotes the minimum value of the set (K_1, K_2), a result originating from the geometric constriction in ballistic thermal conductors mentioned above. Note that equation (2) has taken into account the classical contact resistance
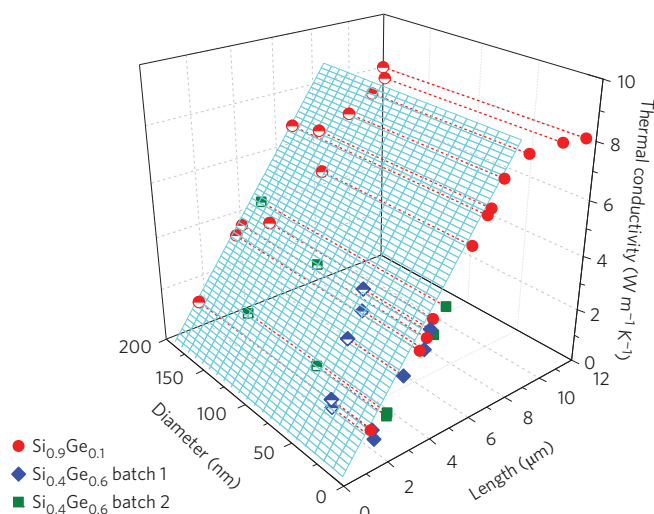
Figure 4 | Length and diameter dependences of κ for SiGe nanowires. The data projected to the κ versus L plane are denoted as solid symbols. Data that show ballistic thermal conduction all fall on a cyan plane. Notably, although the thermal conductivities of SiGe nanowires are strongly correlated with the lengths, they are weakly dependent on the diameters.

so the K_{total} should never exceed $K_1 K_2/(K_1 + K_2)$ for two diffusive conductors connected in series. Therefore, any violations of the inequality of the diffusive thermal conductors in equation (2) will be evidence of ballistic thermal conduction.

Figure 3a,b presents representative SEM images taken when two mechanically touching SiGe nanowires were rubbed, pressed or rotated against one another using a manipulator (Supplementary Section S7, Fig. S6). The lengths, diameters and thermal conductances are, respectively, $L_1 \approx L_2 = 3.65$ μm, $d_1 \approx d_2 = 183$ nm and $K_1 \approx K_2 = 2.81 \times 10^{-8}$ W K^{-1}. The corresponding measured values of K_{total} are presented in Fig. 3c,d. At sequence nos 3, 4 and 5, the data clearly exceed the limit predicted by diffusive conductors. This is because the total length ($L_1 + L_2 = 7.3$ μm < 8.3 μm) is within the ballistic transport regime, and the whole system still behaves like a ballistic thermal conductor (with added phonon scattering at the junction). Remarkably, perfect ballistic phonon transmission (that is, $K_{total} = (K_1, K_2)_{min} = 2.81 \times 10^{-8}$ W K^{-1}) is observed at sequence no. 5, indicating that phonon scattering at the junction can be reduced to zero. Figure 3d displays the measured K_{total} of another two SiGe nanowires of dissimilar diameters connected in series (the lengths, diameters and thermal conductances are, respectively, $L_1 = L_2 = 3$ μm, $d_1 = 158$ nm, $d_2 = 140$ nm, $K_1 = 1.96 \times 10^{-8}$ W K^{-1}, $K_2 = 1.53 \times 10^{-8}$ W K^{-1}). Again the data shown in Fig. 3d disobey the inequality of equation (2) for diffusive conductors. Instead, the K_{total} values follow the inequality for ballistic thermal conductors and the largest values (sequence nos 8 and 9 in Fig. 3d) never exceed $(K_1, K_2)_{min}$. Controlled experiments on connecting two Si nanowires in series indeed demonstrate the expected relation for diffusive conductors (Supplementary Section S8). We emphasize that the results shown in Fig. 3 are the first experimental demonstration of non-additive thermal resistances in series, a unique property of ballistic thermal conduction, now realized at room temperature.

Despite the presence of defects, impurities or variations in composition (shown in Fig. 1c–j), the ballistic thermal conduction shown in Fig. 2 is known to be immune to these perturbations. Furthermore, it is also insensitive to surface roughness. As demonstrated in Fig. 4, although the thermal conductivity of SiGe nanowires is strongly correlated with L, it is weakly dependent on diameter ($\Delta\kappa/(\kappa_{bulk}d) < 5.1 \times 10^{-4}$ nm^{-1}). In contrast, due to the pronounced surface scatterings in Si nanowires and Ge

nanowires, their thermal conductivities decrease rapidly with reducing diameter ($\Delta\kappa/(\kappa_{bulk}d) = 2.3 \times 10^{-3}$ nm^{-1} for Si nanowires and $\Delta\kappa/(\kappa_{bulk}d) = 2.2 \times 10^{-3}$ nm^{-1} for Ge nanowires)[23–26]. Apparently, the alloy scattering in SiGe nanowires filters out most fragile high-frequency phonons, and the remaining low-frequency phonons are insensitive to surface scattering. In fact, the low-frequency phonons are also insensitive to phonon–phonon interactions or external strain, which manifests in the absence of the Umklapp process in the temperature dependence of κ (Supplementary Section S9) and in insensitivities to external strain (Supplementary Section S10). It should be noted that $\kappa < 1$ W m^{-1} K^{-1} when $L < 1$ μm, so the results are consistent with those of granular SiGe (with added complex effects from contact thermal resistance in the granular systems), as studied previously[3,27].

We note that recent works on SiGe nanowires of similar concentrations reported much smaller thermal conductivities than ours[28,29]. We believe that this is because the oxidized layers on the SiGe nanowires reduce the phonon transmission at the contacts. Indeed, we have found that when the oxidized layers are thicker than 8 nm, the measured thermal conductivities are much reduced. On the other hand, when the oxidized layers are thinner than 2 nm, all the results reported above are reproducible.

Although, to date, our investigations are limited to nanowires, the alloy scattering effect could exist in other forms of structures or in other material systems. The unprecedented robust ballistic thermal conduction discovered in our model semiconductor system will lead to new avenues for heat wave engineering at room temperature. Furthermore, ballistic thermal conduction should display quantum effects of phonons and may enable new quantum devices operating at terahertz frequencies. Most importantly, SiGe is a material ready to be integrated into existing semiconductor production lines. All innovations and potential applications will encounter minimum integration difficulties when entering future markets.

Methods

Homogeneously alloyed Si$_{1-x}$Ge$_x$ nanowires with $x = 0.1$ and 0.4 were synthesized in a quartz tube furnace using a chemical vapour deposition method. Gold nanoparticles in a colloid solution were first dripped onto cleaned silicon wafers before being loaded into the deposition system. SiH$_4$ (10% diluted in N$_2$) and GeH$_4$ (10% diluted in N$_2$) were used as the precursor gases to initiate growth. The growth temperatures for the Si$_{0.9}$Ge$_{0.1}$ and Si$_{0.4}$Ge$_{0.6}$ nanowires were 1,050 °C and 365 °C, respectively, and the total pressure was maintained at 30 torr during growth.

The thermal conductivity test fixture consisted of two suspended 14 μm × 25 μm silicon nitride (SiN$_x$) membranes, each supported by five 420-μm-long and 2-μm-wide SiN$_x$ beams. A 500-nm-thick SiN$_x$ film was first deposited on a Si substrate using the low-pressure chemical vapour deposition (LPCVD) process. A 30-nm-thick Pt film and 300-nm-thick low-temperature silicon dioxide (LTO) were then deposited on the SiN$_x$ using a sputtering method and LPCVD, respectively. The exposed portion of the LTO film was etched using reactive ion etching (RIE). The patterned LTO was then used as a mask. The exposed Pt film was etched using ion milling or reactive ion etching to make Pt resistors. The photoresist and LTO were subsequently removed, and a photoresist film was then spun on the wafer and patterned to define two membranes and ten SiN$_x$ beams. The exposed SiN$_x$ film was etched by RIE. After removal of the photoresist, the exposed Si region was etched by tetramethylammonium hydroxide (TMAH) and the suspended membranes were released as the Si underneath was etched away.

To measure the thermal conductance K of the nanowire, Joule heating was supplied to the heater and the temperature rises of the heater and sensor were measured. Under steady-state conditions, K can be obtained using the relation

$$K = \frac{P}{\Delta T_H - \Delta T_S}\left(\frac{\Delta T_S}{\Delta T_H + \Delta T_S}\right) \qquad (3)$$

where P is the Joule heating power and ΔT_H and ΔT_S are the temperature increases on the heater and sensor, respectively. Because of the linear relation of resistance with respect to the temperature of the Pt film resistors, the temperature variations of the heater and sensor can be obtained directly by measuring their resistance. The thermal conductivity κ was evaluated by incorporating the length and diameter of the nanowire, as determined by SEM. The temperature dependence of κ was

measured on a temperature-controlled cryostat. All measurements were carried out at a pressure of $<1 \times 10^{-5}$ mbar to eliminate unwanted heat convection.

References

1. Balandin, A. A. Thermal properties of graphene and nanostructured carbon materials. *Nature Mater.* **10,** 569–581 (2011).
2. Chiu, H. Y. *et al.* Ballistic phonon thermal transport in multiwalled carbon nanotubes. *Phys. Rev. Lett.* **95,** 226101 (2005).
3. Zhu, G. H. *et al.* Increased phonon scattering by nanograins and point defects in nanostructured silicon with a low concentration of germanium. *Phys. Rev. Lett.* **102,** 196803 (2009).
4. Bera, C., Mingo, N. & Volz, S. Marked effects of alloying on the thermal conductivity of nanoporous materials. *Phys. Rev. Lett.* **104,** 115502 (2010).
5. Garg, J., Bonini, N., Kozinsky, B. & Marzari, N. Role of disorder and anharmonicity in the thermal conductivity of silicon–germanium alloys: a first-principles study. *Phys. Rev. Lett.* **106,** 045901 (2011).
6. Hu, M., Giapis, K. P., Goicochea, J. V., Zhang, X. & Poulikakos, D. Significant reduction of thermal conductivity in Si/Ge core–shell nanowires. *Nano Lett.* **11,** 618–623 (2011).
7. Yang, J. E., Jin, C. B., Kim, C. J. & Jo, M. H. Band-gap modulation in single-crystalline $Si_{1-x}Ge_x$ nanowires. *Nano Lett.* **6,** 2679–2684 (2006).
8. Chang, H-K. & Lee, S-C. The growth and radial analysis of Si/Ge core–shell nanowires. *Appl. Phys. Lett.* **97,** 251912 (2010).
9. Rego, L. G. C. & Kirczenow, G. Quantized thermal conductance of dielectric quantum wires. *Phys. Rev. Lett.* **81,** 232–235 (1998).
10. Steele, M. C. & Rosi, F. D. Thermal conductivity and thermoelectric power of germanium–silicon alloys. *J. Appl. Phys.* **29,** 1517–1520 (1958).
11. Koh, Y. K. & Cahill, D. G. Frequency dependence of the thermal conductivity of semiconductor alloys. *Phys. Rev. B* **76,** 075207 (2007).
12. Bolotin, K. I., Ghahari, F., Shulman, M. D., Stormer, H. L. & Kim, P. Observation of the fractional quantum Hall effect in graphene. *Nature* **462,** 196–199 (2009).
13. Du, X., Skachko, I., Duerr, F., Luican, A. & Andrei, E. Y. Fractional quantum Hall effect and insulating phase of Dirac electrons in graphene. *Nature* **462,** 192–195 (2009).
14. Prasher, R. Predicting the thermal resistance of nanosized constrictions. *Nano Lett.* **5,** 2155–2159 (2005).
15. Slack, G. A. & Hussain, M. A. The maximum possible conversion efficiency of silicon-germanium thermoelectric generators. *J. Appl. Phys.* **70,** 2694–2718 (1991).
16. Liu, C-K. *et al.* Thermal conductivity of Si/SiGe superlattice films. *J. Appl. Phys.* **104,** 114301 (2008).
17. Minnich, A. J. *et al.* Modeling study of thermoelectric SiGe nanocomposites. *Phys. Rev. B* **80,** 155327 (2009).
18. Meddins, H. R. & Parrott, J. E. Thermal and thermoelectric properties of sintered germanium–silicon alloys. *J. Phys. C* **9,** 1263–1276 (1976).
19. Lu, Q. *et al.* Raman scattering from $Si_{1-x}Ge_x$ alloy nanowires. *J. Phys. Chem. C* **112,** 3209–3215 (2008).
20. Ju, Y. S. & Goodson, K. E. Phonon scattering in silicon films with thickness of order 100 nm. *Appl. Phys. Lett.* **74,** 3005–3007 (1999).
21. Alvarez-Quintana, J., Rodriguez-Viejo, J., Alvarez, F. X. & Jou, D. Thermal conductivity of thin single-crystalline germanium-on-insulator structures. *Int. J. Heat Mass Transf.* **54,** 1959–1962 (2011).
22. Smith, C. G. Low-dimensional quantum devices. *Rep. Prog. Phys.* **59,** 235–282 (1996).
23. Li, D. Y. *et al.* Thermal conductivity of individual silicon nanowires. *Appl. Phys. Lett.* **83,** 2934–2936 (2003).
24. Chen, R. K. *et al.* Thermal conductance of thin silicon nanowires. *Phys. Rev. Lett.* **101,** 105501 (2008).
25. Hochbaum, A. I. *et al.* Enhanced thermoelectric performance of rough silicon nanowires. *Nature* **451,** 163–165 (2008).
26. Wingert, M. C. *et al.* Thermal conductivity of Ge and Ge–Si core–shell nanowires in the phonon confinement regime. *Nano Lett.* **11,** 5507–5513 (2011).
27. Rowe, D. M., Shukla, V. S. & Savvides, N. Phonon-scattering at grain-boundaries in heavily doped fine-grained silicon–germanium alloys. *Nature* **290,** 765–766 (1981).
28. Lee, E. K. *et al.* Large thermoelectric figure-of-merits from SiGe nanowires by simultaneously measuring electrical and thermal transport properties. *Nano Lett.* **12,** 2918–2923 (2012).
29. Yin, L. *et al.* The influence of phonon scatterings on the thermal conductivity of SiGe nanowires. *Appl. Phys. Lett.* **101,** 043114 (2012).

Acknowledgements

Author contributions

T.K.H. conducted the thermal conductivity measurements and analysed the data. H.K.C. and S.C.L. contributed the nanowires. S.C.L. and M.W.C. performed the TEM characterizations. C.W.C. initiated the project, supervised it, and wrote the paper. All authors discussed the results and commented on the manuscript.

Additional information

Supplementary information is available in the online version of the paper. Reprints and permissions information is available online at www.nature.com/reprints. Correspondence and requests for materials should be addressed to C.W.C.

Competing financial interests

The authors declare no competing financial interests.

Supplementary Information: Observation of room temperature ballistic thermal conduction persisting over 8.3 micrometers in SiGe nanowires

Tzu-Kan Hsiao, Hsu-Kai Chang, Sz-Chian Liou, Ming-Wen Chu, Si-Chen Lee, and Chih-Wei Chang

S1. Thermal conductivity measurements employing heater/sensor pads. Figure S1a shows the schematic of the thermal conductivity test fixture. It consists of two suspended 14μm × 25μm silicon nitride (SiN$_x$) membranes each supported by five 420μm-long and 2μm-wide SiN$_x$ beams. Patterned Pt film resistors were fabricated on the suspended SiN$_x$ membranes to serve as independent heaters and sensors. To measure the thermal conductance (K) of the nanowire, a dc current was applied to the heater to generate Joule heating power P. The power dissipated on the heater (P_1) raised its temperature by ΔT_H while the other portion of the Joule heat (P_2) flowed through the sample and raised the temperature of the sensor by ΔT_S. Under steady state, we have the following relation:

$$\begin{cases} P = P_1 + P_2 \\ P_1 = K_A \Delta T_H \\ P_2 = K_B \Delta T_S = K\left(\Delta T_H - \Delta T_S\right) \end{cases} \quad \text{(S1)}$$

where $K_A \sim K_B$ is the total thermal conductance of the supporting SiN$_x$ beams and K is the thermal conductance of the sample. From Eq. (S1), K can be obtained as follows:

$$K = \frac{P}{\Delta T_H - \Delta T_S}\left(\frac{\Delta T_S}{\Delta T_H + \Delta T_S}\right) \quad \text{(S2)}$$

Due to the linear relation of the Pt film resistors versus temperature (shown in Fig. S1b), the corresponding temperature variations on the heater and sensor can be determined via measuring their resistance changes. The thermal conductivity κ was evaluated by incorporating the length (L) and the diameter (d) of the nanowire determined by SEM, i.e.

$$\kappa = K\left(\frac{4L}{\pi d^2}\right) \quad \text{(S3)}$$

We have noted that because the nanowires do not exhibit uniform diameters, the averaged d used in Eq. S3 contributes most of the uncertainties in determining κ.
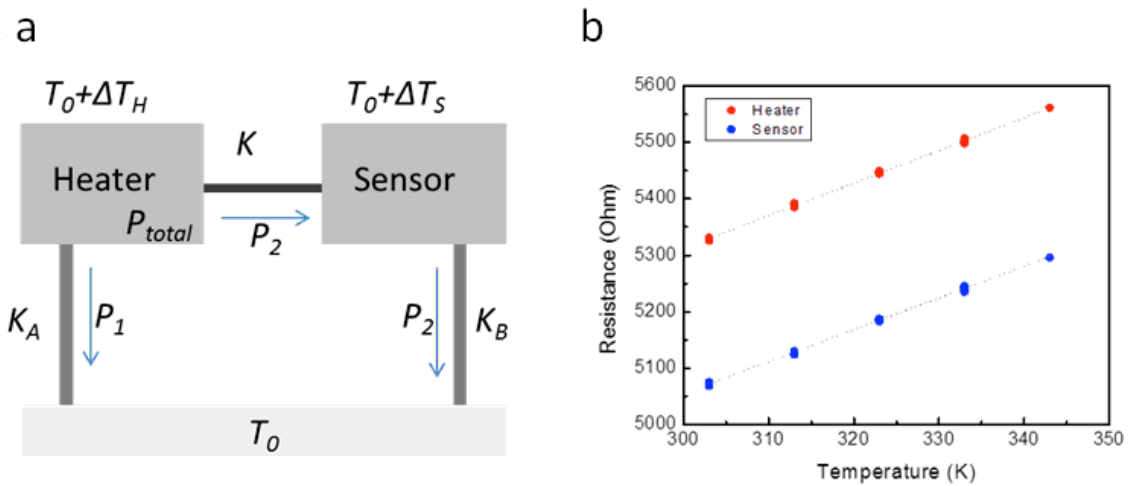
Figure S1. Thermal conductivity measurements employing heater/sensor pads. (a) Schematic of the heat flow diagram of the thermal conductivity test fixture. When a Joule heating power P was generated in the heater, the temperature of the heater was raised by ΔT_H while a portion of the Joule heat (P_2) flowed through the sample and raised the temperature of the sensor by ΔT_S. The thermal conductance of the sample (K) can be determined via Eq. (S1) and (S2). (b) The resistance vs. temperature of the heater and the sensor.

S2. Structures of $Si_{0.4}Ge_{0.6}$ nanowires. To investigate the structure of the $Si_{0.4}Ge_{0.6}$ nanowires, we note that the scattering of electrons by defects lies primarily at the forward direction and is highly angular dependent. Therefore, changing the collection angles of the HAADF images will allow us to identify the distributions of structural variations other than defects. We have found that the stripe patterns are still visible when increasing the HAADF collection inner radius from 46 mrad (Fig. S2a) to 129 mrad (Fig. S2b). The result indicates that, in addition to defects, there are accompanied composition variations along the axial axis of the nanowire. Further evidence for the composition variations can be seen from the EDS spectra shown in Fig. S2c. The EDS spectra acquired at different positions of the $Si_{0.4}Ge_{0.6}$ nanowire clearly reveal the correlation between the intensity contrast and the composition variation. The corresponding stoichiometric analyses suggest that the composition varies from $Si_{0.4}Ge_{0.6}$ to $Si_{0.33}Ge_{0.67}$. We thus conclude that the observed stripe patterns in the $Si_{0.4}Ge_{0.6}$ nanowire are due to defects along with composition variations.

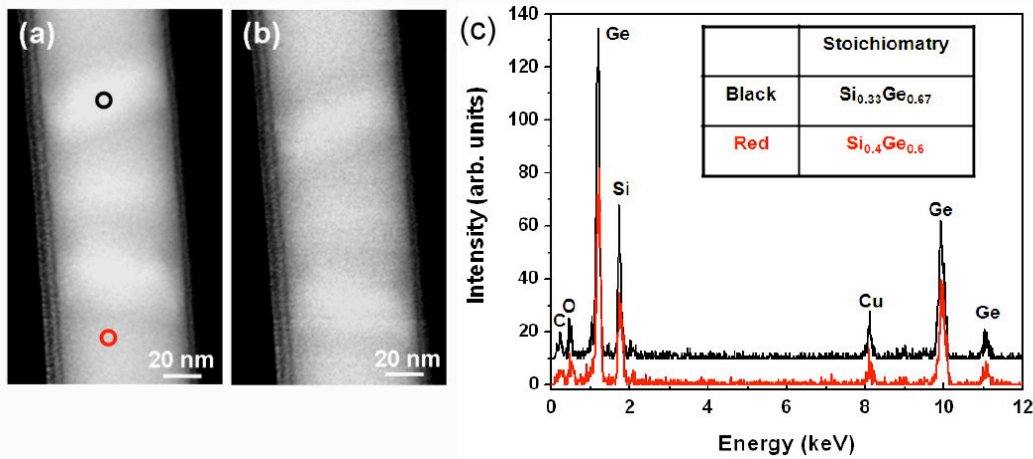**Figure S2. Elemental analyses of $Si_{0.4}Ge_{0.6}$ nanowires.** HAADF images of a $Si_{0.4}Ge_{0.6}$ nanowire acquired with collection inner radius (a) 46 mrad and (b) 129 mrad. (c) STEM–EDS spectra acquired on the $Si_{0.4}Ge_{0.6}$ nanowires with the electron probe positioned at the black and red circles of (a). Inset table in (c) shows the corresponding Si and Ge concentration determined by EDS analysis.

S3. Contact resistance of individual SiGe nanowire. Figure S3 shows the length dependence of thermal resistance ($1/K$) of an individual SiGe nanowire. The data display a transition from ballistic to diffusive transport at $L \sim 8\mu m$. Extrapolating the data in the diffusive regime ($L > 8\mu m$) to $L \rightarrow 0$ (red dotted line) indicates that classical contact thermal resistance contributes $\sim 10\%$ of the total thermal resistance at $L = 8\mu m$. On the other hand, extrapolating the data in the ballistic regime ($L < 8\mu m$) to $L \rightarrow 0$ (cyan dotted line) indicates constant (quantum) contact thermal resistance.
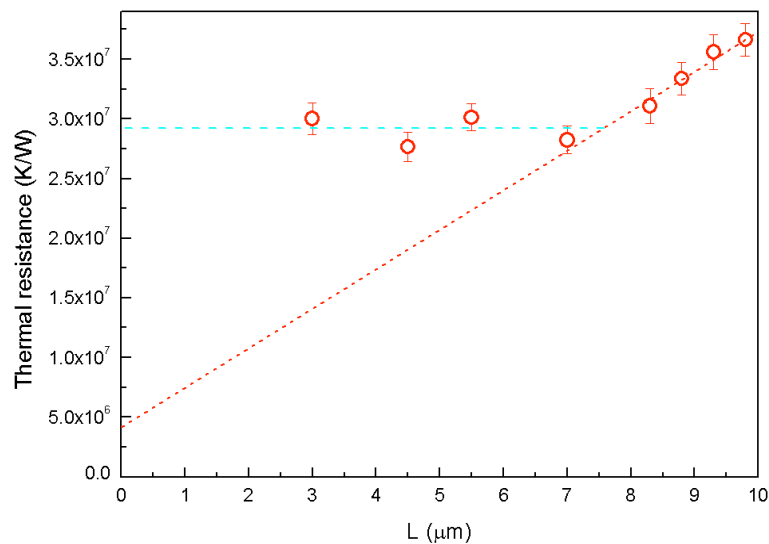

Figure S3. $1/K$ vs. L for a SiGe nanowire. The red-dotted line and the cyan-dotted line denote the extrapolated contact thermal resistance in the diffusive and ballistic transport regimes, respectively.

S4. Phonon spectrum of SiGe. We have estimated that only 0.04% of the excited phonon modes contributing to the heat transfer process in the SiGe nanowire. To determine the corresponding phonon frequency, we have integrated the phonon density of states to 0.04% of the excited phonon modes (as shown in Fig. S4) and found that phonons with frequencies less than 0.3THz are the dominant heat carriers in SiGe nanowires[1].
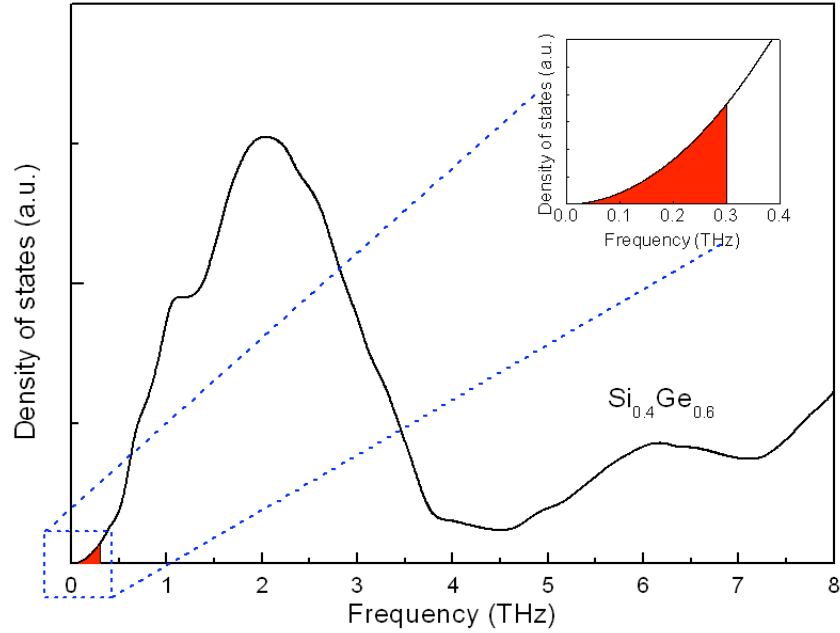

Figure S4. Phonon density of states of Si$_{0.4}$Ge$_{0.6}$. Integrating phonon density of states to 0.04% of the excited phonon modes (shown in the red area) of a Si$_{0.4}$Ge$_{0.6}$ nanowire. The corresponding phonon frequency is found to be less than 0.3THz (shown in the inset). The phonon density of states is obtained from Q. Lu et al[1].

S5. Comparison between Si, Ge, carbon nanotubes, and SiGe. Table S1 compares $C_a v_a$ (obtained from the slope of the κ vs. L relation at the ballistic phonon regimes), $C_{bulk}v_{bulk}$ (from experimental data)[1-3], l (directly obtained from the experimental κ vs. L relation), l' (estimated from the conventional method based on the kinetic theory), and the ratio of excited phonon modes contributing to the heat conduction ($N_p/N_{total} = C_a v_a/C_{bulk}v_{bulk}$) in Si, Ge, carbon nanotubes, and SiGe. It can be seen that although $C_{bulk}v_{bulk}$ of SiGe is not much different from those of other materials, its $C_a v_a$ is three orders of magnitude lower than those of others materials, resulting in only 0.04% of excited phonon modes carrying out the heat conduction in SiGe.

Table S1. Comparison of various parameters between Si, Ge, carbon nanotubes, and SiGe. C_{bulk}'s of Si, Ge, and SWCNT are from Ref. [2], [3], and [4], respectively. v_{bulk}'s of Si, Ge, and SWCNT are from Ref. [5] and [6], respectively. The mass density of SWCNT is from Ref. [7]. The experimental the κ vs. L relations of Si, Ge, and SWCNT are from Ref. [8], [9], and [10], respectively.

	Si	Ge	Carbon nanotube	SiGe
$C_a v_a$ (W/K-m^2)	2.3×10^9	1.6×10^9	2.2×10^9	2.9×10^6
$C_{bulk} v_{bulk}$ (W/K-m^2)	9.3×10^9	5.9×10^9	1.2×10^{10}	7.0×10^9
l (nm)	140	100	909	8300
l' (nm)	45.6	25.5	160	4.3
N_p/N_{total}	24%	27%	18%	0.04%

S6. Estimates on the quantum channel and the phonon wavelengths. Because the total thermal conductance of a SiGe nanowire is proportional to its cross-sectional area and the number of channels (N) of quantum conductance ($K_Q \sim 10^{-10}$ W/K at 300K), from $K/A = \kappa/L = 9.5 \times 10^5$ W/K-m^2 = NK_Q/A, we obtain the averaged area occupied by each quantum channel $A/N \sim 100$nm^2. Furthermore, N can be obtained via integrating the density of states:

$$N = \int_0^{k_{max}} D(k)d^2k = \frac{Ak_{max}^2}{4\pi^2} \tag{S4}$$

where $k_{max} = 2\pi/\lambda_{min}$ denotes the maximum wave vector (or equivalently, the shortest wavelength λ_{min}) of phonons that carry out the heat conduction in a SiGe nanowire. From Eq. (S4), we obtain $\lambda_{min} \sim 10$nm and maximum frequency of the phonons $f \sim v_a/\lambda_{min} = 0.4$THz, consistent with earlier estimates based on $C_a/C_{bulk} = 0.04\%$.

S7. Thermal conductivity measurements employing a tungsten tip and a heater. Figure S5 displays the experimental configuration for the experiment shown in Fig. 3. Here a constant power (P) was supplied to the heater and the temperature rise of the heater before (ΔT_b) and after (ΔT_a) connecting the nanowires was measured. Because the thermal conductance of the tungsten tip is $\sim 10^4$ higher than the nanowire, it functions like a heat sink for the system. The thermal conductance (K) of the nanowire can be obtained via

$$K = P\left(\frac{1}{\Delta T_a} - \frac{1}{\Delta T_b}\right) \tag{S5}$$

We then measured the K of the system when we rubbed, pressed, or rotated the two

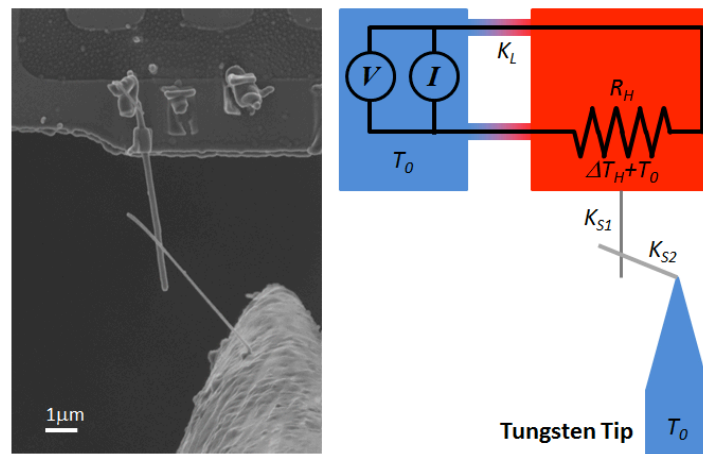nanowires against each other using a piezo-driven manipulator. The results are shown in Fig. 3.

Figure S5. Thermal conductivity measurements employing a tungsten tip and a heater. (Left) An SEM image of the experimental setup where one end of a nanowire is anchored to a microfabricated heater and another nanowire is attached to a tungsten tip serving as a heat sink. (Right) The corresponding thermal circuit diagram where the heat sink is maintained at temperature T_0 and the Joule heating raises the temperature of the heater to $\Delta T_H + T_0$. The difference of ΔT_H before and after connecting the nanowires is measured so as to determine the total thermal conductance (K) of the sample.
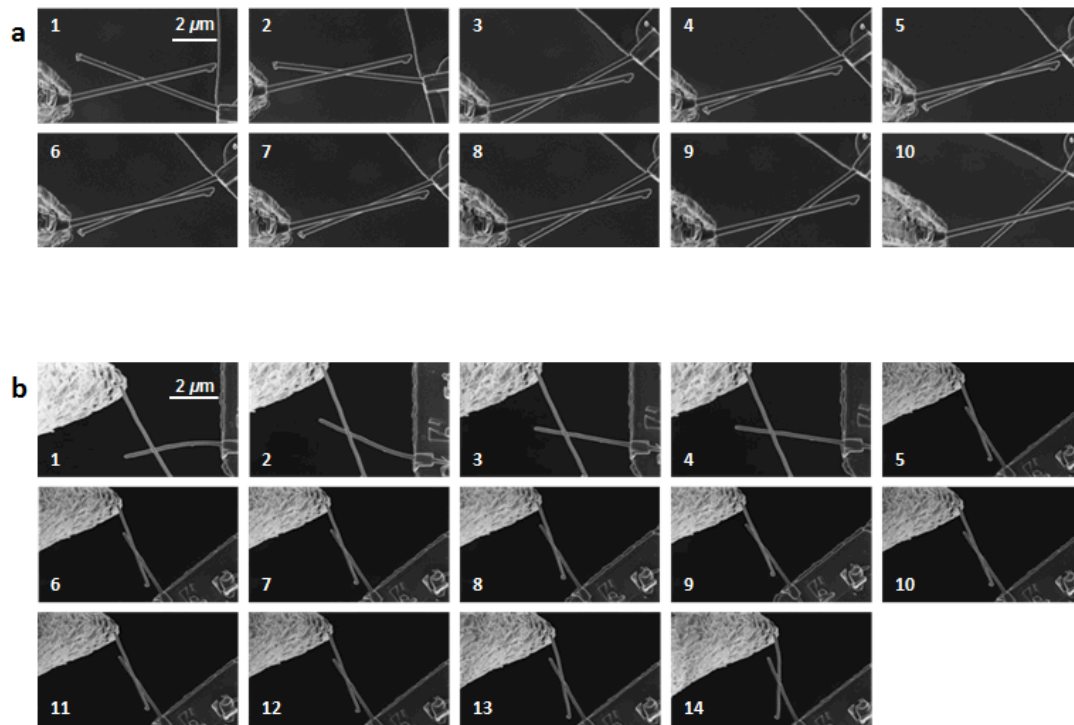

Figure S6. SEM images for the sequences shown in Fig. 3. SEM images shown in (a) and (b) correspond to the sequence shown in Fig. 3c and d, respectively.

S8. Controlled experiments on two Si nanowires connected in series. Figure S7 shows the measured total thermal conductance K_{total} as we rubbed, pressed, or rotated the two mechanically-touched Si nanowires against each other using a manipulator (the lengths, diameters, and thermal conductances are respectively L_1 =4.5μm, L_2 = 2μm, d_1 = 53nm, d_2 = 64nm, K_1 = 3×10^{-9} W/K, K_2 = 8.1×10^{-9} W/K). Because the lengths of the Si nanowires are much larger than the phonon mean free path (l), the system is within the diffusive thermal conduction regime. As expected, due to the nonzero contact thermal resistance at the junction, the measured K_{total} never exceed the value $K_1K_2/(K_1+K_2)$ predicted for two diffusive conductors connected in series.
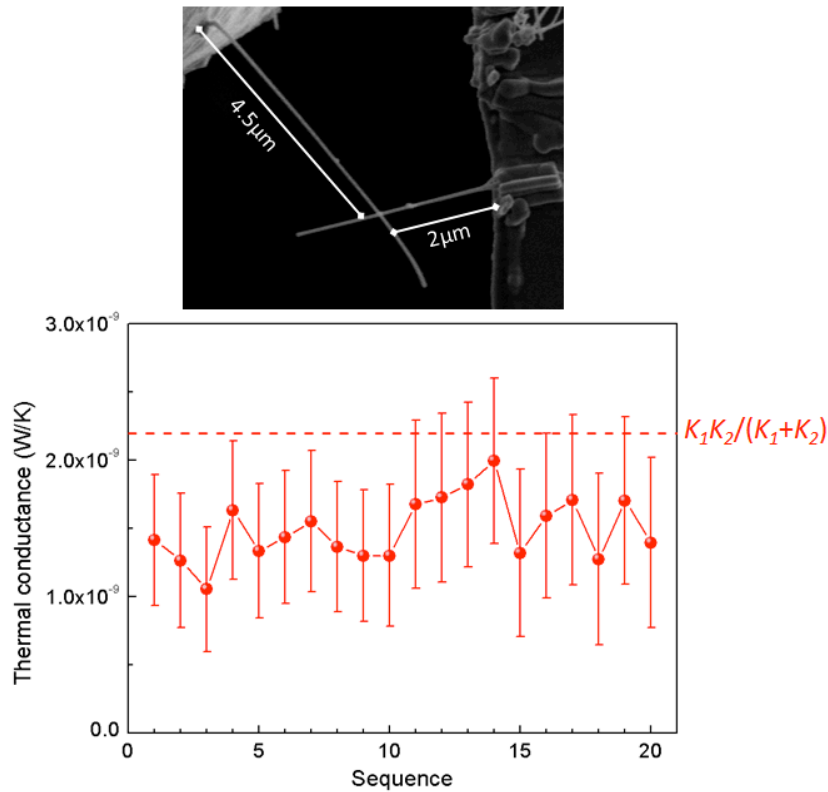

Figure S7. Controlled experiment on Si nanowires. (Upper) A SEM image of two Si nanowires connected in series. (Lower panel) The measured K_{total} when the junction thermal resistance is sequentially varied by rubbing, pressing, or rotating the Si nanowires against each other using a manipulator. The red dashed line denotes the maximum K_{total} allowed by Eq. (2) in the paper for diffusive thermal conductors.

S9. Temperature dependence of κ. Figure S8 shows the temperature dependences of thermal conductivity ($\kappa(T)$) of two SiGe nanowires at 30-300K temperature range. Comparing with $\kappa(T)$'s of bulk Si or Ge, the $\kappa(T)$'s of SiGe nanowires display weakly temperature-dependent behavior. In addition, the absence of umklapp process features

in the $\kappa(T)$'s suggests that phonon-phonon interactions are negligible and is consistent with the observed ballistic phonon behavior. Apparently, alloy scatterings, which are not sensitively dependent on temperature, dominate the heat transfer phenomena of SiGe nanowires throughout the investigated temperature range and remain effective in localizing majorities of phonons with frequency higher than 0.4THz.
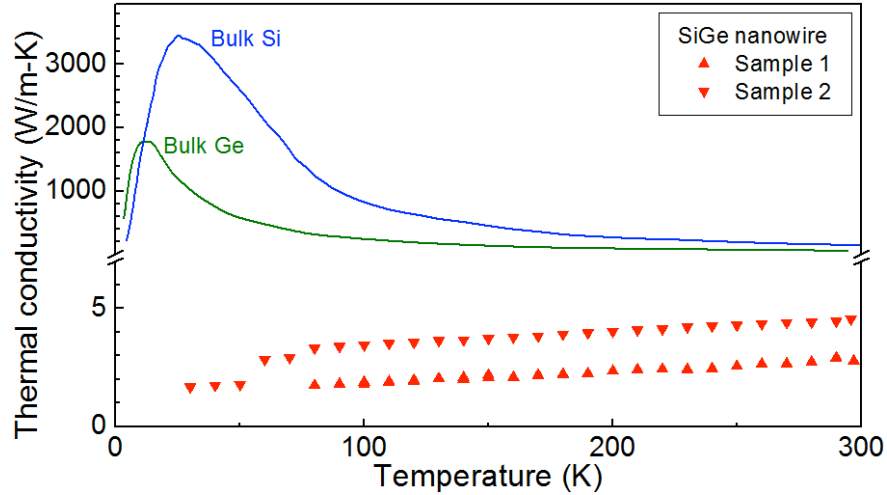

Figure S8. Temperature dependent thermal conductivity ($\kappa(T)$) of SiGe nanowires. $\kappa(T)$'s of two SiGe nanowires (up and down triangles) display weak temperature dependences and absences of umklapp process. $\kappa(T)$'s of bulk Si (blue line) and bulk Ge (green line) are also shown for comparison.

S10. Insensitivities of κ to external strain. The extraordinary properties of the low-frequency ballistic phonons can be further demonstrated in another phenomenon shown in Fig. S9 where in-situ K measurements were carried out when SiGe nanowires underwent structural bending. Under external bending stresses, the SiGe nanowires can be deformed into various shapes shown in Fig. S9. To quantify the structural deformation, we define a dimensionless quantity by dividing l by the smallest radius of curvature (R_c) observed in the SEM images. Surprisingly, l/R_c respectively reaches 6.3 and 13.4 at frame 4 for two samples without observing any changes in K. Because low frequency phonons are barely scattered by local defects or dislocations, we attribute the unusual phenomena to the alloy scattering effect that filters out most fragile high-frequency phonons and guides the robust acoustic phonons propagating through the SiGe nanowire without dissipation. Interestingly, the effect remains robust before structural failures eventually happen on the nanowire, as shown in Fig. S9.
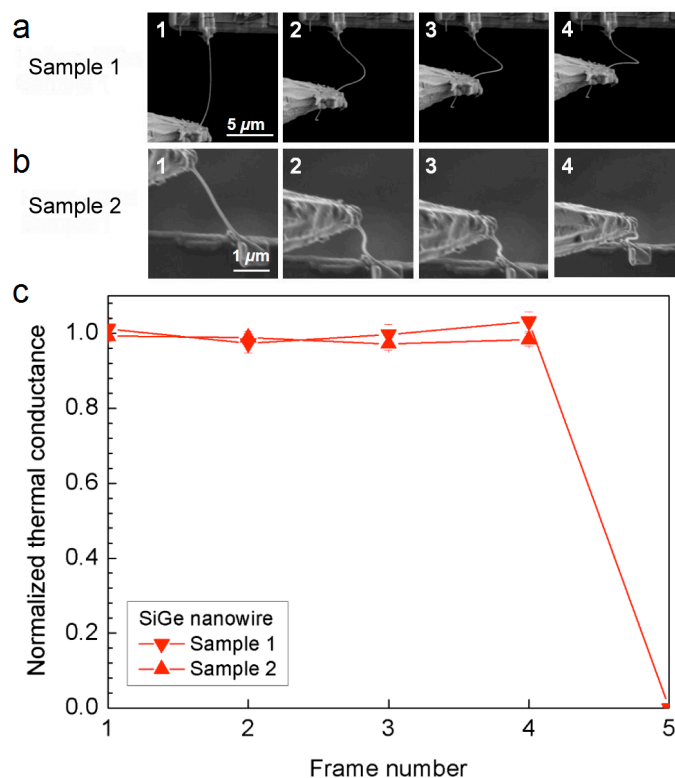
Figure S9. Insensitivities of κ to external strain. (a) Representative SEM images of SiGe nanowire (a) Sample 1 and (b) Sample 2 under external stress applied by a tungsten tip. (c) The corresponding in-situ thermal conductance measurements when two samples undergo structural bending. The last data point at frame 5 denotes the thermal conductance dropping to zero when the nanowire was broken.

Supplementary information references

1   Lu, Q. *et al.* Raman scattering from $Si_{1-x}Ge_x$ alloy nanowires. *J. Phys. Chem. C* **112**, 3209-3215 (2008).

2   Levinshtein, M. E. & Rumyantsev, S. L. in *Handbook Series On Semiconductor Parameters*   1-32.

3   Vorobyev, L. E. in *Handbook Series On Semiconductor Parameters* 33-57.

4   Hone, J., Batlogg, B., Benes, Z., Johnson, A. T. & Fischer, J. E. Quantized phonon spectrum of single-wall carbon nanotubes. *Science* **289**, 1730-1733 (2000).

5   McSkimin, H. J. Measurement of Elastic Constants at Low Temperatures by Means of Ultrasonic Waves--Data for Silicon and Germanium Single Crystals, and for Fused Silica. *J. Appl. Phys.* **24**, 988-997 (1953).

6   Osman, M. A. & Srivastava, D. Molecular dynamics simulation of heat pulse

propagation in single-wall carbon nanotubes. *Phys. Rev. B* **72**, 125413 (2005).

7   Guanghua, G., Tahir, Ç. & William, A. G., III. Energetics, structure, mechanical and vibrational properties of single-walled carbon nanotubes. *Nanotechnology* **9**, 184 (1998).

8   Ju, Y. S. & Goodson, K. E. Phonon scattering in silicon films with thickness of order 100 nm. *Appl. Phys. Lett.* **74**, 3005-3007 (1999).

9   Alvarez-Quintana, J., Rodriguez-Viejo, J., Alvarez, F. X. & Jou, D. Thermal conductivity of thin single-crystalline germanium-on-insulator structures. *Int. J. Heat Mass Tran.* **54**, 1959-1962 (2011).

10   Chiu, H. Y. *et al.* Ballistic phonon thermal transport in multiwalled carbon nanotubes. *Phys. Rev. Lett.* **95**, 226101 (2005).